

# Dalton Transactions

Accepted Manuscript



This is an *Accepted Manuscript*, which has been through the Royal Society of Chemistry peer review process and has been accepted for publication.

*Accepted Manuscripts* are published online shortly after acceptance, before technical editing, formatting and proof reading. Using this free service, authors can make their results available to the community, in citable form, before we publish the edited article. We will replace this *Accepted Manuscript* with the edited and formatted *Advance Article* as soon as it is available.

You can find more information about *Accepted Manuscripts* in the [Information for Authors](#).

Please note that technical editing may introduce minor changes to the text and/or graphics, which may alter content. The journal's standard [Terms & Conditions](#) and the [Ethical guidelines](#) still apply. In no event shall the Royal Society of Chemistry be held responsible for any errors or omissions in this *Accepted Manuscript* or any consequences arising from the use of any information it contains.

# Electronic tuning of $\text{Mo}_2(\text{thioamidate})_4$ complexes through $\pi$ -system substituents and *cis/trans* isomerism

Brian S. Dolinar and John F. Berry\*

Department of Chemistry, University of Wisconsin-Madison, 1101 University Avenue, Madison, WI, 53704.

Email: berry@chem.wisc.edu

## Abstract

We report an exploration of the coordination chemistry of a systematic series of cyclic thioamidate ligands with the quadruply-bonded  $\text{Mo}_2^{4+}$  core. In addition to the S and N donor atoms that bind to Mo, the ligands utilized in this study have an additional O or S atom in conjugation with the thioamidate  $\pi$  system. The preparation of four new  $\text{Mo}_2$  complexes is described, and these compounds are characterized by X-ray crystallography, NMR and UV-vis spectroscopy, electrochemistry, and DFT calculations. These complexes provide a means to interrogate the electronics of  $\text{Mo}_2(\text{thioamidate})_4$  systems. Notably, we describe the first two examples of  $\text{Mo}_2(\text{thioamidate})_4$  complexes in their *cis*-2,2-regioisomer. By varying the  $\pi$ -system substituent and regioisomerism of these compounds, the electronics of the dimolybdenum core is shown to be altered with varying degrees of effect. Cyclic voltammetry results show that changing the  $\pi$ -system substituent from O to S results in an increase in the  $\text{Mo}_2^{4+/5+}$  oxidation potential by 170 mV. Changing the arrangement of ligands around the dimolybdenum core from *trans*-2,2 to *cis*-2,2 slightly weakens the metal-ligand bonds, raising the oxidation potential by a more modest 30-100 mV. MO diagrams of each compound derived from DFT calculations support these conclusions as well; the identity of the  $\pi$ -system substituent alters the  $\delta$ - $\delta^*$  (HOMO-LUMO) gap by up to 0.4 eV, whereas regioisomerism yields smaller changes in the electronic structure.

## Introduction

Metal-metal bonded bimetallic paddlewheel compounds of the transition metals have been a rich source of diverse chemistry for the past 50 years,<sup>1</sup> and are currently of interest with regards to their reactivity<sup>2</sup>, catalytic,<sup>3</sup> electronic,<sup>4</sup> photophysical,<sup>5</sup> and structural properties.<sup>6</sup> Most notable among these compounds are a plethora of  $\text{Mo}_2^{4+}$  paddlewheel complexes supported by carboxylate, amidate, and amidinate equatorial bridging ligands that have been synthesized, and whose properties have been studied in great detail.<sup>1</sup> The difference in the basicity of these ligands has been demonstrated to tune properties such as the  $\text{Mo}_2^{4+/5+}$  redox potential and the HOMO/LUMO gap.<sup>7</sup> In contrast, only a small handful of  $\text{Mo}_2$  compounds containing thioamidate bridging ligands have been reported.<sup>7-8</sup> Thioamidate ligands have been shown to have electronic properties intermediate between carboxylates, amidates, and amidinates.<sup>7</sup> Yet, there has been no systematic study of  $\text{Mo}_2(\text{thioamidate})_4$  compounds to determine how changes to the ligand architecture or ligand arrangement in the complex affect the electronics of the  $\text{Mo}_2$  core.

The thioamide ligands monothiosuccinimide (HSNO5), dithiosuccinimide (HSNS5), monothiopiperidinone (HSNO6), and 2,6-dithiopiperidinone (HSNS6) used in this study are shown in Scheme 1. These ligands consist of a thioamide group that can readily bind to the  $\text{Mo}_2$  core as well as an O or S atom in conjugation with the thioamidate unit that can alter the electronics of the ligand. The ligands that contain oxygen as the  $\pi$ -substituent in principle could bind to  $\text{Mo}_2$  either through S or O, but we have shown previously that these ligands preferentially bind through S in agreement with predictions from hard-soft acid-base (HSAB) theory.<sup>8a</sup>

In addition to changes to the ligand composition, the electronics of Mo<sub>2</sub> paddlewheel complexes can be altered by changing the arrangement of the ligands around the Mo<sub>2</sub> core. In bridging ligands like amidates and thioamidates that contain two different donor atoms, four different regioisomers are possible as shown in Scheme 2.<sup>7</sup> For analogous Mo<sub>2</sub>(amidate)<sub>4</sub> complexes the *trans*-2,2 arrangement predominates, but a number of compounds with *cis*-2,2 arrangements are known.<sup>7,9</sup> The few Mo<sub>2</sub>(thioamidate)<sub>4</sub> compounds that are known adopt the *trans*-2,2 arrangement around the Mo<sub>2</sub> core almost exclusively, where two thioamidate ligands *trans* to each other are oriented in the same direction along the Mo≡Mo vector, while the other two thioamidate ligands are oriented in the opposite direction.<sup>7-8</sup> The *trans*-2,2 arrangement is the thermodynamically favored regioisomer, presumably due to sterics.<sup>7</sup> Previous experiments with the HSNOX ligands have yielded compounds with the *trans*-2,2-Mo<sub>2</sub>(SNOX)<sub>4</sub> (Scheme 3, compounds **1a** and **1b**) when the deprotonated ligand was allowed to react with Mo<sub>2</sub>(OAc)<sub>4</sub> or Mo<sub>2</sub>(TFA)<sub>4</sub>. However, when the thermodynamics of the reaction were altered by inclusion of a Lewis acidic cation as a template, the 4,0 arrangement was observed.<sup>8a</sup>

We now report the synthesis and characterization of four new dimolybdenum paddlewheel complexes that contain thioamidate supporting ligands including the first two examples of *cis*-2,2 isomers: *trans*-2,2-Mo<sub>2</sub>(SNS5)<sub>4</sub> (**2**), *trans*-1,1-Mo<sub>2</sub>(OAc)<sub>2</sub>(SNS6)<sub>2</sub> (**3**), *cis*-2,2-Mo<sub>2</sub>(SNO5)<sub>4</sub> (**4a**), and *cis*-2,2-Mo<sub>2</sub>(SNO6)<sub>4</sub> (**4b**). Within this series of compounds it is possible now to examine the role that  $\pi$ -substituent identity (O vs S) and regioisomerism (*cis* vs *trans*) play in the electronic structure of the Mo<sub>2</sub>(thioamidate)<sub>4</sub> core. These compounds are studied structurally using X-ray crystallography, and their electronics are probed by electrochemistry, UV-vis spectroscopy, and DFT calculations.

## Experimental

## General

All synthetic manipulations were carried out under an inert N<sub>2</sub> atmosphere using standard Schlenk and glovebox techniques unless otherwise stated. CH<sub>2</sub>Cl<sub>2</sub> and 1,2-C<sub>2</sub>H<sub>4</sub>Cl<sub>2</sub> were dried sequentially over molecular sieves and CaH<sub>2</sub> and distilled under N<sub>2</sub> prior to use. Hexane was dried using a Vacuum Atmospheres solvent purification system and degassed with N<sub>2</sub> prior to use. Pyridine was dried sequentially over molecular sieves and barium oxide. It was then distilled under N<sub>2</sub> and stored in a glovebox prior to use. All other commercial reagents were used as received without further purification. Acetic acid, acetic anhydride, Lawesson's reagent, glutarimide, succinimide, P<sub>2</sub>S<sub>5</sub>, lithium hexafluorophosphate, tetrabutyl ammonium hexafluorophosphate, trifluoroacetic acid and molybdenum carbonyl were purchased from Sigma Aldrich. Molybdenum acetate (Mo<sub>2</sub>(OAc)<sub>4</sub>) was synthesized from molybdenum carbonyl, acetic acid, and acetic anhydride.<sup>10</sup> Molybdenum trifluoroacetate (Mo<sub>2</sub>(TFA)<sub>4</sub>) was synthesized from Mo<sub>2</sub>(OAc)<sub>4</sub> and trifluoroacetic acid.<sup>11</sup> Monothiosuccinimide (HSNO5) and dithiosuccinimide (HSNS5) were prepared from succinimide and P<sub>2</sub>S<sub>5</sub>.<sup>12</sup> 2,6-dithiopiperidinone (HSNS5) was prepared from glutarimide and Lawesson's reagent.<sup>13</sup> 6-thio-2-piperidinone (HSNO6) was prepared from glutarimide and either Lawesson's reagent or P<sub>2</sub>S<sub>5</sub>.<sup>12-13</sup> Elemental analysis was carried out by Midwest Microlabs in Indianapolis, IN, USA. Mass spectrometry data were recorded at the Mass Spectrometry Facility of the Chemistry Instrument Center of the University of Wisconsin—Madison. Matrix-assisted laser desorption/ionization (MALDI) mass spectra were obtained using a Bruker REFLEX II spectrometer equipped with a 337 nm laser, a reflectron, delayed extraction, and a time-of-flight (TOF) analyzer or a Bruker ULTRAFLEX spectrometer equipped with a SmartBeam laser. The IR spectra were taken on a Bruker

TENSOR 27 spectrometer using ATR techniques.  $^1\text{H}$  and  $^{13}\text{C}$  NMR spectra were recorded on either a Bruker AC-360 or Bruker Avance-500 spectrometer.

*trans*-2,2-tetrakis(dithiosuccinimidato)dimolybdenum(II) (*trans*-2,2-Mo<sub>2</sub>(SNS5)<sub>4</sub>) (**2**).

A 50 mL Schlenk flask was charged with 84.7 mg HSNS5 (0.645 mmol) and 101.0 mg Mo<sub>2</sub>(TFA)<sub>4</sub> (0.1591 mmol). These were dissolved in 20 mL MeOH, immediately giving an orange solution. Then, 150  $\mu\text{L}$  NEt<sub>3</sub> (1.1 mmol) was added *via* syringe, and a purple-brown solid immediately precipitated. The reaction mixture was heated to 71° C for 24 h. and subsequently cooled to room temperature. The purple-brown microcrystalline solid was collected by filtration, washed with 2 x 25 mL MeOH, and dried under vacuum overnight. Yield 99.1 mg (87.4%). X-ray quality crystals were obtained by slow diffusion of hexanes into a CH<sub>2</sub>Cl<sub>2</sub> solution of **2**.

Anal. calcd. for C<sub>17</sub>H<sub>18</sub>Cl<sub>2</sub>Mo<sub>2</sub>N<sub>4</sub>S<sub>8</sub> (Mo<sub>2</sub>(SNS5)<sub>4</sub>·CH<sub>2</sub>Cl<sub>2</sub>): C, 25.60%; H 2.27%; N, 7.02%.

Found C, 25.79%; H, 2.24%; N, 6.93%.  $^1\text{H}$  NMR (500 MHz, CDCl<sub>3</sub>)  $\delta$  3.64 (m, 2H) 3.36 (m, 2H).  $^{13}\text{C}$  NMR (125 MHz, CDCl<sub>3</sub>)  $\delta$  224.58, 215.55, 45.15, 42.20. IR (ATR, cm<sup>-1</sup>) 2911 vw, 1421 w, 1372 m 1302 s, 1210 vs (C=S), 1175 s, 1111 m, 1035 vw, 975 vw, 937 vw, 787 vw.

MALDI-TOF Mass Spectrum (m/z) 712 [M]<sup>+</sup>. UV-vis (CH<sub>2</sub>Cl<sub>2</sub>,  $\lambda_{\text{max}}$ , nm [ $\epsilon$ (M<sup>-1</sup>, cm<sup>-1</sup>)]): 375 [17,000], 505 [5,100]

*trans*-1,1-bis(2,6-dithiopiperidinonato)bis(acetato)dimolybdenum(II) (Mo<sub>2</sub>(SNS6)<sub>2</sub>(OAc)<sub>2</sub>) (**3**)

A 100 mL Schlenk flask was charged with 1.06 g 2,6-dithiopiperidinone (7.30 mol) dissolved in 30 mL anhydrous THF. After cooling this solution to -78° C, 4.6 mL (7.4 mmol) of a 1.6 M solution of MeLi in Et<sub>2</sub>O was added *via* syringe, and the solution turned a brilliant orange color and evolved a gas. Once gas evolution ceased, the solution was allowed to warm to room temperature over a period of 30 minutes. Then, this solution was transferred *via* cannula to a flask containing 1.57 g Mo<sub>2</sub>(OAc)<sub>4</sub> (3.67 mmol). The reaction mixture immediately became a

deep shade of emerald green, and a similarly colored green precipitate formed. The reaction mixture was allowed to stir at room temperature for 5.5 h. The resulting solid was collected by filtration in air and was washed with methanol (3 x 50 mL). The solid was then dissolved in CH<sub>2</sub>Cl<sub>2</sub> by continuous extraction under nitrogen. The CH<sub>2</sub>Cl<sub>2</sub> was then removed under vacuum. The resulting green solid was washed with hexanes and collected by gravity filtration in air. Yield: 553 mg (25.3%). Suitable crystals for X-ray diffraction were obtained by slow diffusion of hexanes into a saturated solution of Mo<sub>2</sub>(SNS)<sub>2</sub>(OAc)<sub>2</sub> in CH<sub>2</sub>Cl<sub>2</sub>. Anal. calcd. for C<sub>14</sub>H<sub>18</sub>Mo<sub>2</sub>N<sub>2</sub>O<sub>4</sub>S<sub>4</sub>: C, 28.10%; H, 3.03%; N, 4.68%. Found: C, 27.97%; H, 3.09%; N, 4.61%. <sup>1</sup>H NMR (CDCl<sub>3</sub>, 300 MHz, ppm): δ 3.35 (t, *J* = 6.3 Hz, 2H, CSCH<sub>2</sub>CH<sub>2</sub>CH<sub>2</sub>CS), 2.94 (t, *J* = 6.3 Hz, 2H, CSCH<sub>2</sub>CH<sub>2</sub>CH<sub>2</sub>CS), 2.87 (s, 3H, CH<sub>3</sub>CO<sub>2</sub>), 2.10 (p, *J* = 6.3 Hz, 2H, CSCH<sub>2</sub>CH<sub>2</sub>CH<sub>2</sub>CS). MALDI-TOF Mass Spectrum (*m/z*): 598.8 *m/z* [M]<sup>+</sup>. IR (ATR, cm<sup>-1</sup>): 2933 vw, 2851 vw, 1487 w, 1433 m, 1412 m, 1362 s, 1331 s, 1266 s, 1238 m, 1203 w, 1165 w, 1102 vs (C=S), 1034 w, 1020 m, 961 m, 921 m, 906 m, 852 w, 791 m, 738 w, 731 w, 669 s, 632 w, 628 w. UV-Vis (CH<sub>2</sub>Cl<sub>2</sub>, λ<sub>max</sub>, nm [ε(M<sup>-1</sup>, cm<sup>-1</sup>)]): 371 [17000], 477 [1200], 648 [2400]. *cis*-2,2-tetrakis(monothiosuccinimidato)dimolybdenum(II) (*cis*-2,2-Mo<sub>2</sub>(SNO<sub>5</sub>)<sub>4</sub>)(**4a**).

A 50 mL Schlenk flask was charged with 196 mg HSNO<sub>5</sub> (1.70 mmol) and 268 mg Mo<sub>2</sub>(TFA)<sub>4</sub> (0.422 mmol). These were dissolved in 20 mL MeOH. Then, 350 μL NEt<sub>3</sub> (2.5 mmol) was added, and immediately the solution became a brilliant orange color. Within a minute, a red-orange precipitate formed. The reaction was then heated to 71° C for 16 hours, and then cooled to room temperature. The solid was collected by filtration, washed with 3 x 25 mL MeOH and dried overnight under vacuum. Yield: 215 mg (78.6%). Suitable crystals for X-ray diffraction were obtained by dissolving the compound in CH<sub>2</sub>Cl<sub>2</sub> and layering with hexanes. Crystals of the bis-methanol solvate could be obtained in the same manner except with the

omission of the vacuum drying step of the procedure. Anal. calcd. for  $C_{20}H_{20}S_4N_4O_4Mo_2$ : C, 29.63%; H, 2.49%; N, 8.64%. Found C, 29.62%; H, 2.54%; N, 8.38%.  $^1H$  NMR (500 MHz,  $CDCl_3$ )  $\delta$  3.52 (dt,  $J=20, 5$  Hz, 4H,  $OCCH_2CHHCS$ ), 3.47 (dt,  $J=20, 5$  Hz, 4H,  $OCCH_2CHHCS$ ), 2.81 (t,  $J=5$  Hz, 8H,  $OCCH_2CH_2CS$ ).  $^{13}C$  NMR (500 MHz,  $CDCl_3$ )  $\delta$  216.31, 187.38, 39.48, 32.43. IR (ATR,  $cm^{-1}$ ): 2938 (vw), 1722 (m) (C=O), 1430 (w), 1411 (w), 1400 (s), 1242 (m), 1200 (vs) (C=S), 1115 (w), 1020 (m), 1000 (w), 916 (w), 811 (w), 668 (w). MALDI-TOF MS (m/z): 649 [ $M^+$ ]. UV-vis ( $CH_2Cl_2$ ,  $\lambda$ (nm) [ $\epsilon$ ( $M^{-1}cm^{-1}$ )]): 410 [8560], 498 [1100].

*cis*-2,2-tetrakis(monothiopiperidinonato)dimolybdenum(II) (*cis*-2,2- $Mo_2(SNO_6)_4$ , **4b**)

A 50 mL Schlenk flask was charged with 298 mg  $HSNO_6$  (2.31 mmol) and 440 mg LiCl (10.4 mmol) dissolved in 20 mL THF. A separate 100 mL Schlenk flask was charged with 367 mg  $Mo_2(TFA)_4$  (0.578 mmol) and 460 mg LiCl (10.85 mmol) dissolved in 20 mL THF. To the ligand solution was added 500  $\mu$ L  $NEt_3$ . Then, both of these solutions were cooled to  $-78^\circ C$ . The ligand solution was added to the metal solution *via* cannula. Immediately, the reaction changed to a deep, red-violet color. After 30 s - 1 min, the THF solvent was removed under vacuum. The residue was extracted by 20 mL  $CH_2Cl_2$  at room temperature. Upon layering with hexanes, a red-orange solid appeared. The solid was then washed with 3 x 20 mL degassed  $H_2O$  and 3 x 30 mL  $Et_2O$ . The remaining solid was recrystallized from 1,2- $C_2H_4Cl_4$  by layering with  $Et_2O$ , yielding an orange powder. Yield: 34.8 mg (8.56%). Suitable crystals for X-ray diffraction were obtained by further recrystallization of the powder from 1,2- $C_2H_4Cl_2$  layered with hexanes. The low yield of this reaction precluded characterization by elemental analysis.  $^1H$  NMR ( $CDCl_3$ , 500 MHz, ppm)  $\delta$  3.42 (dt,  $J=18, 5.5$  Hz, 4H,  $SCCHHCH_2CH_2CO$ ), 3.29 (ddd,  $J=18, 8.5, 5$  Hz, 4H,  $SCCHHCH_2CH_2CO$ ), 2.59 (dt,  $J=18, 5.5$  Hz, 4H,  $SCCH_2CH_2CHHCO$ ), 2.49 (ddd,  $J=18, 9.5, 5.5$  Hz, 4H,  $SCCH_2CH_2CHHCO$ ), 2.13 (m, 8H,  $SCCH_2CH_2CH_2CO$ ).  $^{13}C$  NMR ( $CDCl_3$ ,

125 MHz, ppm)  $\delta$  208.4, 177.7, 39.6, 32.1, 21.6. IR (ATR,  $\text{cm}^{-1}$ ) 1687 m (C=O), 1441 m, 1404 s, 1331 m, 1256 vs, 1240 vs, 1177 vs, 1119 vs, 1054 vw, 976 m, 941 w, 913 w, 885 w, 847 w, 765 w, 664 m, 645 m, MALDI-TOF Mass Spectrum ( $m/z$ ) 704  $[\text{M}]^+$  UV-vis ( $\text{CH}_2\text{Cl}_2$ ,  $\lambda_{\text{max}}$ , nm [ $\epsilon$  ( $\text{M}^{-1}$ ,  $\text{cm}^{-1}$ )]): 449[6910], 502 [2100].

### X-ray Crystallography

Suitable single crystals of **2**· $\text{CH}_2\text{Cl}_2$ , **4a**· $\text{CH}_2\text{Cl}_2$ , and **4b**·1,2- $\text{C}_2\text{H}_4\text{Cl}_2$  and twinned crystals for **3** and **4a**·2MeOH were selected under oil and ambient conditions. The crystals were attached to the tip of a MiTeGen MicroMount and mounted in a stream of cold nitrogen at 100(1) K (**2**· $\text{CH}_2\text{Cl}_2$ , **3**, **4a**· $\text{CH}_2\text{Cl}_2$ , **4a**·2MeOH, **4b**·1,2- $\text{C}_2\text{H}_4\text{Cl}_2$ ) or 200(1) K (**4a**·2MeOH) and centered in the X-ray beam using a video monitoring system. The crystal evaluation and data collection were performed on a Bruker Quazar SMART APEX-II diffractometer with Mo  $\text{K}\alpha$  ( $\lambda = 0.71073$  Å) (**2**· $\text{CH}_2\text{Cl}_2$ , **3**, **4a**· $\text{CH}_2\text{Cl}_2$ , **4a**·2MeOH (100 K), **4b**·1,2- $\text{C}_2\text{H}_4\text{Cl}_2$ ) or Cu  $\text{K}\alpha$  ( $\lambda = 1.54178$  Å) (**4a**·2MeOH (200 K)) radiation. The data were collected using a routine to survey an entire sphere of reciprocal space and were indexed by the SMART program.<sup>14</sup> The structures were solved *via* direct methods and refined by iterative cycles of least-squares refinement on  $F^2$  followed by difference Fourier synthesis using the SHELX2013 program.<sup>15</sup> In structures **4a**·2MeOH (100 K) and **4a**·2MeOH (200 K), the MeOH hydrogen atom of the major component was located from the Fourier difference map and refined independently. All other hydrogen atoms were included in the final structure factor calculation at idealized positions and were allowed to ride on the neighboring atoms with relative isotropic displacement coefficients. The unit cell for **4a**·2MeOH was also determined at several temperatures between 100K to 200K using Cu  $\text{K}\alpha$  ( $\lambda = 1.54178$  Å) radiation.

The details concerning X-ray crystallographic structure solutions and refinement for **2**· $\text{CH}_2\text{Cl}_2$ ,

**3**, **4a**·CH<sub>2</sub>Cl<sub>2</sub>, **4a**·2MeOH (100 K), **4a**·2MeOH (200 K), and **4b**·1,2-C<sub>2</sub>H<sub>4</sub>Cl<sub>2</sub> are tabulated in Table 1. For each structure, the model was refined to a low wR2 value (< 0.15 for all data in each case).

### Electrochemistry

Cyclic voltammetry was performed for compounds **2**, **4a**, and **4b** on solutions of 1 mM analyte and 100 mM electrolyte (NBu<sub>4</sub>PF<sub>6</sub>) in CH<sub>2</sub>Cl<sub>2</sub> at 20°C using a standard glassy carbon electrode for the working electrode, a platinum wire for the auxiliary electrode, and an Ag/Ag<sup>+</sup> electrode as the reference electrode. All electrochemical potentials were internally referenced to the ferrocene/ferrocenium couple. The voltammetry was performed in the range of 1200 mV to -1200 mV at a scan rate of 100 mV/s.

### Calculations

Restricted Kohn-Sham geometry optimization and single-point calculations on those optimized geometries were carried out on **1a**, **1b**, **2**, **4a**, and **4b** through the ORCA electronic structure package using the B3LYP functional.<sup>16</sup> The def3 basis sets from the Karlsruhe group were used,<sup>17</sup> which are automatically recontracted in ORCA for use with the scalar relativistic zeroth-order regular approximation (ZORA). Optimized structures for these compounds were calculated using initial atomic coordinates taken from the crystal structures and then optimized until the energy change between steps was less than 10<sup>-6</sup> Hartree. All calculations were optimized with a Grid4 optimization grid and tight SCF convergence criteria.

## Results and Discussion

### Syntheses

We recently reported the preparation of compounds **1a** and **1b** by reaction of Mo<sub>2</sub>(TFA)<sub>4</sub> with HSNO<sub>5</sub> and Mo<sub>2</sub>(OAc)<sub>4</sub> with HSNO<sub>6</sub>, respectively, in pyridine.<sup>8a</sup> However, in the course of

our work here, we have determined that the previously reported preparation of **1a** yields a mixture containing predominantly **1a** with small amounts of other isomeric impurities.<sup>18</sup>

Compound **2** was synthesized in good yield (87.4%) by the reaction of  $\text{Mo}_2(\text{TFA})_4$  with a stoichiometric amount of HSNS5 and an excess of  $\text{NEt}_3$  in MeOH as shown in Scheme 3. The compound is not very soluble in MeOH and precipitates directly from the reaction mixture upon addition of  $\text{NEt}_3$ . Compound **2** is more soluble in halogenated solvents, such as  $\text{CH}_2\text{Cl}_2$  and  $\text{CHCl}_3$ , and is somewhat soluble in MeCN. It can be easily purified by washing with MeOH and recrystallizing from  $\text{CH}_2\text{Cl}_2$  by layering with hexanes.

Compound **3** was synthesized in moderate yield (25.3 %) by reacting  $\text{Mo}_2(\text{OAc})_4$  with a stoichiometric amount of LiSNS6. Immediately a green solid precipitates upon addition of the deprotonated ligand to  $\text{Mo}_2(\text{OAc})_4$ . Preparation of the tetra-substituted complex,  $\text{Mo}_2(\text{SNS6})_4$ , was attempted in numerous ways, including using a synthetic method analogous to that of **2** as well as forcing conditions such as excess ligand and reaction temperatures as high as  $140^\circ\text{C}$  in diglyme. In our hands, these reactions routinely yielded a mixture of di-, tri-, and tetra-substituted compounds as evidenced by MALDI-MS, but these were not separable. It is likely that the sterics of the HSNS6 ligand make the tri- and tetra-substituted compounds thermodynamically disfavored in comparison to the di-substituted compound.

Compound **4a** forms under similar reaction conditions as **2**, using the HSNO5 ligand in place of HSNS5. In this case, the *cis*-2,2 regioisomer is favored instead of the *trans*-2,2 isomer, and can be synthesized in 78.6% isolated yield. In comparison with the synthesis of **1a**, it is evident that changing the solvent from pyridine to methanol provides selectivity for one regioisomer over the other.

Formation of tetra-substitued **4a** requires the use of  $\text{Mo}_2(\text{TFA})_4$  as a starting material and an external base, such as  $\text{NEt}_3$ , in order achieve reaction completion. Using  $\text{Mo}_2(\text{OAc})_4$  as a starting material and omitting the base causes the reaction not to go to completion. Rather, the reaction stops at the disubstituted species (Figure S1), which is the SNO5 analogue of **3**.

The preparation of **4b** is not nearly as facile as that of **4a**. When the same reaction conditions for preparing **4a** are used with the HSNO6 ligand, the result is predominantly *trans*-2,2- $\text{Mo}_2(\text{SNO6})_4$ , compound **1b**. Compound **4b** can be isolated as a minor, kinetic product from the reaction of  $\text{Mo}_2(\text{TFA})_4$  with HSNO6 and  $\text{NEt}_3$  in THF at  $-78^\circ\text{C}$  (Scheme 3). Indeed, the major product from this reaction has also proven to be **1b**, but the two isomers can be separated by washing with water, in which **1b** is soluble, and ether followed by extraction with 1,2- $\text{C}_2\text{H}_4\text{Cl}_2$ .

Compound **4b** is soluble in halogenated solvents such as  $\text{CH}_2\text{Cl}_2$ , 1,2- $\text{C}_2\text{H}_4\text{Cl}_2$ , and chloroform as well as alcohols. It is sparingly soluble in acetonitrile, water, toluene, and diethyl ether. It is insoluble in hexanes.

### NMR Spectroscopy

The *trans*-2,2 SNX5 complexes have idealized  $\text{D}_{2d}$  point symmetry and have mirror planes coplanar with the plane of the ligands, which makes both geminal methylene protons chemically equivalent. In *cis*-2,2- $\text{Mo}_2(\text{SNO5})_4$ , the symmetry is  $\text{C}_{2h}$ , and the mirror plane passes between adjacent ligands, rather than through the ligands. Molecules of *cis*-2,2- $\text{Mo}_2(\text{SNO6})_4$ , while not rigidly held to  $\text{C}_{2h}$  symmetry, can nonetheless adopt a conformation that has  $\text{C}_{2h}$  symmetry in solution. For both cases of the *cis*-2,2 regioisomer, this leads us to expect that the geminal methylene protons are not chemically equivalent, which distinguishes the *cis*-2,2 complexes from their corresponding *trans*-2,2 complexes.

The  $^1\text{H}$  NMR spectrum of **2** consists of two signals at 3.64 and 3.36 ppm. These signals show no sign of geminal coupling that would be indicative of chemically independent methylene protons. Thus, this spectrum is consistent with the *trans*-2,2 regioisomer of  $\text{Mo}_2(\text{SNS5})_4$ .

The  $^1\text{H}$  NMR spectrum of **4a** consists of three signals that show coupling in an  $\text{ABX}_2$  type pattern, and it is distinct from the spectrum of **1a** based on this coupling.<sup>18</sup> There are two partially overlapping, yet chemically distinct signals around 3.5 ppm, which show a strong geminal coupling constant ( $J=20$  Hz). These signals are assigned to two protons on the methylene group closest to the C=S bond based on where those protons appear in the spectrum of the free HSNO5 ligand. The other signal around 2.8 ppm belongs to the  $\text{CH}_2$  adjacent to the C=O bond. These two protons coincidentally have the same chemical shift. This spectrum is only consistent with the *cis*-2,2 regioisomer of  $\text{Mo}_2(\text{SNO5})_4$ .

Likewise, the  $^1\text{H}$  NMR spectrum of **4b** shows 6 distinct signals, one for each of the 6 ligand protons. There are two signals at 3.42 and 3.25 ppm that correspond to the methylene protons adjacent to the C=S group, as well as two signals at 2.59 and 2.49 ppm that correspond to the methylene protons adjacent to the C=O group. A group of overlapping signals at 2.13 ppm corresponds to the methylene spacer. Like the  $^1\text{H}$  NMR spectrum of **4a**, this spectrum is consistent with the *cis*-2,2 ligand arrangement.

### X-ray Crystallography

The relevant bond distances for structures of **2**, **3**, **4a**, and **4b** are listed in Table 2.

Structures **2**· $\text{CH}_2\text{Cl}_2$ , **3**, **4a**· $\text{CH}_2\text{Cl}_2$ , and **4b**·1,2- $\text{C}_2\text{H}_4\text{Cl}_2$  all crystallized in the monoclinic space group  $P2_1/c$ . Crystals of **4a**·2MeOH were formed by recrystallizing solid **4a** that had precipitated from the reaction mixture without first drying it *in vacuo*. Crystals of **4a**·2MeOH

were found to undergo a phase transition and were either monoclinic  $P2_1/c$  or triclinic  $P\bar{1}$  depending on the temperature at which the data were collected (*vide infra*).

The X-ray crystal structures of **2**, **3**, **4a**·CH<sub>2</sub>Cl<sub>2</sub>, **4a**·2MeOH, and **4b**·1,2-C<sub>2</sub>H<sub>4</sub>Cl<sub>2</sub> (Figures 1-5, respectively) each confirmed the identification of the regioisomers determined by NMR spectroscopy (*vide supra*). **2**·CH<sub>2</sub>Cl<sub>2</sub> is in the *trans*-2,2 arrangement, **3** is the *trans*-1,1 isomer,<sup>19</sup> **4a**·CH<sub>2</sub>Cl<sub>2</sub> is the *cis*-2,2 isomer, and **4b**·1,2-DCE, is also the *cis*-2,2 isomer.

There is significant variation in the Mo≡Mo bond length among compounds **2-4**. Compounds **2**, **3** and **4b**, have Mo≡Mo bond lengths of 2.1242(6) Å, 2.108(2) Å, and 2.1061(2) Å, respectively, which are typical for Mo≡Mo quadruple bonds. Compound **4a**, on the other hand, has a Mo≡Mo bond length of 2.145(2) Å, which is longer than most Mo≡Mo bonds, especially those containing thioamidate bridging ligands.<sup>1,7-8</sup> The arrangement of molecules in the unit cell of **4a** results in an oxygen atom from one molecule being in close proximity (2.607(3) Å) to the axial position of an adjacent molecule of **4a**. This close Mo···O interaction likely elongates the Mo≡Mo bond slightly by donating some electron density into the σ-antibonding orbital of the Mo<sub>2</sub> unit.

The crystallographically determined metal-ligand bond distances are less varied than the Mo≡Mo bond distances for complexes **2 - 4**. The Mo–N bond distances range from 2.155[6] Å to 2.166[3] Å, and the Mo–S distances range from 2.4790[4] Å to 2.499[2] Å, both of which are typical for Mo<sub>2</sub>(thioamidate) complexes. The Mo–N bond distances for complexes **4a** and **4b** are slightly, yet statistically significantly longer than those of **1a** and **1b** by ~0.02 Å and 0.01 Å, respectively.<sup>8a</sup> The pendant oxygen atoms of the ligand are much closer to each other in the *cis*-2,2 complexes (O···O distance: **4a** = 3.28 Å, **4b** = 2.98 Å) than they are in the corresponding *trans*-2,2 complexes (O···O distance: **1a** = 4.60 Å, **1b** = 3.28 Å), which results in this slight

elongation of the *cis*-2,2 Mo–N and, to a lesser extent, the Mo–S bond distances. This metal-ligand bond weakening in the *cis*-2,2 isomer will be further discussed in relation to the observed trends in the electrochemical data (*vide infra*).

Compound **4a** also crystallizes as a MeOH solvate, **4a**·2MeOH. In this solvate, the MeOH molecules occupy the axial position of **4a**, but the Mo···O distances are long, 2.653(9) Å. Like its unsolvated counterpart, this long Mo···O axial interaction likely elongates the Mo≡Mo bond (2.153[2] Å). The crystallographic data also show that the alcohol group of the MeOH molecule forms a hydrogen bond with the carbonyl group of a coordinated SNO5 ligand. In the *cis*-2,2 isomer, the ligand arrangement allows the MeOH to form this close contact with the Mo<sub>2</sub> core as well as the hydrogen bond, whereas in the *trans*-2,2 isomer, the arrangement of the ligands sterically prevents MeOH from forming a close contact with the Mo<sub>2</sub> core, and thus prevent this interaction. This set of interactions likely causes the of the *cis*-2,2 regioisomer to be the thermodynamically favored product over the *trans*-2,2 regioisomer when the formation of **4a** is carried out in MeOH.

### Phase Change of **4a**·MeOH

Two complete crystallographic data sets were taken on crystals of **4a**·2MeOH, one at 100 K and one at 200 K. At 200 K, the unit cell was determined to be a monoclinic *P* cell with the dimensions  $a = 9.0133(5)$  Å,  $b = 14.716(1)$  Å,  $c = 10.0976(7)$  Å,  $\alpha = \gamma = 90^\circ$ ,  $\beta = 111.403(4)^\circ$ , and at 100 K, the unit cell was determined to be a triclinic *P* cell with the dimensions  $a = 8.990(3)$  Å,  $b = 14.717(7)$  Å,  $c = 10.048(4)$  Å,  $\alpha = 89.646(17)^\circ$ ,  $\beta = 112.528(13)^\circ$ ,  $\gamma = 88.73(2)^\circ$ . The 200 K structure has an asymmetric unit that consists of 1/2 of one molecule of **4a** with a MeOH molecule occupying the axial position. A crystallographic center of symmetry lies at the

midpoint of the Mo≡Mo bond. At 100 K, the asymmetric unit consists of two symmetry independent half molecules of **4a** with corresponding MeOH molecules in each axial position.

The unit cell was measured at various temperatures between 200 K and 100 K. Figure 6 shows the deviation of the unconstrained  $\alpha$  angle from  $90^\circ$ . At temperatures  $> 160$  K, the  $\alpha$  angle is very close to  $90^\circ$ . However, between 160 K and 150 K, the deviation of  $\alpha$  from  $90^\circ$  rapidly increases to  $0.25^\circ$ . From the inflection point of this graph, the transition temperature was determined to be  $153 \pm 1$  K. In addition to the loss of symmetry from monoclinic P to triclinic P, twinning occurs upon cooling the crystal below 153 K. The two twin components are related by

a 2-fold rotation around the  $b$  axis (twin law:  $\begin{bmatrix} \bar{1} & 0 & 0 \\ 0 & 1 & 0 \\ 0 & 0 & \bar{1} \end{bmatrix}$ ). The twinning reverses itself upon warming. The same crystal was able to undergo this phase transition several times.

A side-by-side comparison of the 200 K and 100 K structures suggests a reason for the phase change (Figure 7). At 200 K, the MeOH in the axial position of the Mo<sub>2</sub> complex is positionally disordered such that 86% of the time it forms a hydrogen bond with atom O1 and 14% of the time it forms a hydrogen bond with atom O2 where O1 and O2 are the oxygen atoms of adjacent SNO5 ligands. At 100 K, one of the symmetry independent molecules of **4a** has a MeOH that is disordered much like the 200 K structure, while the other independent molecule of **4a** has an ordered MeOH that forms a hydrogen bond with only one ligand oxygen atom. This difference in MeOH hydrogen bonding behavior prevents these two symmetry independent molecules from being related to each other by a two-fold screw axis as they are in the 200 K structure. The ordering of one of the MeOH molecules upon cooling further supports the suggestion that hydrogen bonding plays an important role in the formation of the *cis*-2,2 isomer of Mo<sub>2</sub>(SNO5)<sub>4</sub>.

## Electrochemistry

The electrochemical oxidation potentials of compounds **2**, **4a**, and **4b** are presented in Table 3 alongside the *trans*-2,2-Mo<sub>2</sub>(SNO<sub>5</sub>)<sub>4</sub> and *trans*-2,2-Mo<sub>2</sub>(SNO<sub>6</sub>)<sub>4</sub> complexes. For each of these compounds, the CV showed an irreversible signal between 400 mV and 700 mV vs. Fc/Fc<sup>+</sup>, which is attributed to the Mo<sub>2</sub><sup>4+/5+</sup> oxidation potential and is among the highest oxidation potentials reported for this redox process in Mo<sub>2</sub>(thioamidate)<sub>4</sub> complexes (literature range: 92 - 520 mV vs. Fc/Fc<sup>+</sup>).<sup>7,8a,8c,8d</sup> While these waves are irreversible, preventing an accurate determination of the E<sub>1/2</sub> of the redox couple, the anodic peak potentials for these compounds can be compared since they were taken at the same scan rate of 100 mV/s. The *trans*-2,2 complexes have the lowest potential; the *cis*-2,2 complexes have oxidation potentials that are approximately 30 - 100 mV higher than their *trans*-2,2 counterparts. The oxidation potential of **2** has a potential that is 170 mV higher than the highest of the Mo<sub>2</sub>(SNOX)<sub>4</sub> complexes (Figure 8).

This trend in oxidation potentials is related to the degree to which the equatorial thioamidate ligands can donate electron density to the Mo<sub>2</sub> core in order to stabilize the [Mo<sub>2</sub>]<sup>5+</sup> oxidation state. In the *trans*-2,2 complexes, the ligands are the least sterically crowded, and thus are able to form the strongest bonds with the Mo<sub>2</sub> core. The slightly weaker metal-ligand bonds in the *cis*-2,2 complexes are not able to stabilize the [Mo<sub>2</sub>]<sup>5+</sup> core as well as those of the *trans*-2,2 complex, and may be responsible for the slight increase in oxidation potential.

Despite being a *trans*-2,2 complex, **2** has by far the highest oxidation potential of all the compounds compared here. The main difference between **2** and the other compounds is that it bears SNS rather than SNO ligands. Thus, the inherent electronic differences between SNS and SNO ligands must be taken into account. In the SNS ligand, the valence 3p orbitals of the pendant S atom do not overlap as well in a π sense with the 2p orbitals of the adjacent C atom as

does the O 2p orbital of the SNO ligand. Thus there is less C=S double bond character in the SNS ligands than there is with the C and O atoms of the SNOX complexes. If we keep in mind the limiting resonance structures, **A** and **B**, shown in Scheme 4, we would expect the zwitterionic resonance structure (**B**) for the SNS5 ligand to be more predominant than in the SNO ligand. Thus, SNS5 is less  $\pi$ -basic than its SNO counterpart, which results in a higher oxidation potential for the Mo<sub>2</sub> complex.

### Electronic Spectra

The UV-vis spectra of **1-4** are shown overlaid in Figure 9, and the spectral data are summarized in Table 4. For Mo<sub>2</sub>(SNOX)<sub>4</sub> complexes **1a**, **4a**, and **4b**, the spectra each consist of one band around 410-450 nm with a high extinction coefficient ( $> 5,000 \text{ M}^{-1} \text{ cm}^{-1}$ ), and a second peak at  $\sim 500$  nm with an extinction coefficient that is roughly an order of magnitude less intense. Because of its intensity, the former band is attributed to a Mo  $\delta$  to ligand  $\pi^*$  charge transfer band, and the latter may be attributed to a  $\delta$ - $\delta^*$  transition based on comparison with UV-vis spectra of similar Mo<sub>2</sub> complexes.<sup>7</sup> Complex **1b** has only one MLCT band at 460 nm that likely masks the  $\delta$ - $\delta^*$  transition.

The spectra of the SNSX complexes **2** and **3** both contain very intense bands around 375 nm with an extinction coefficient around  $17,000 \text{ M}^{-1} \text{ cm}^{-1}$ , attributed to a ligand  $\pi$ - $\pi^*$  transition. These spectra also contain the same Mo  $\delta$  to ligand  $\pi^*$  transition as the Mo<sub>2</sub>(SNOX)<sub>4</sub> complexes, but these occur much lower in energy (505 and 648 nm, respectively) than those of **1a**, **1b**, **4a**, and **4b**. Compound **3** also contains an easily distinguished  $\delta$ - $\delta^*$  transition at 477 nm that is close in energy to those of the SNOX complexes. From these data, it is evident that the MLCT moves to a dramatically lower energy when S is substituted for O as the  $\pi$ -system substituent. However,

changing the regioisomerism from *trans*-2,2 to *cis*-2,2 has only minimal effect on the electronic spectra of these complexes.

### DFT Calculations

DFT calculations were used to investigate the nature of the Mo≡Mo bonding manifold in complexes **1**, **2**, and **4**. The optimized Mo≡Mo, Mo–N, and Mo–S bond distances are given in Table 2 alongside the crystallographically determined experimental values. The calculated geometries are very close to the experimental geometries. The Mo≡Mo bond distances are calculated to be shorter than the crystallographic values with differences ranging from ~0.023 Å for **4b** to 0.063 Å for **4a**. For the former, this is an acceptable difference. However, for the latter, this difference is large enough to cause concern.

The calculated structure of **4a** does not take packing effects into account in determining the Mo≡Mo bond length. The calculated structure of **4a**·2MeOH, which includes both axial MeOH molecules, has a Mo≡Mo bond length of 2.131 Å, which is much closer to the experimentally determined value for **4a** (2.153[2] Å), supporting our earlier premise that the weak Mo···O axial interaction can serve to elongate a Mo≡Mo bond.

The relative thermodynamic energies of **1a** and **4a** as well as **1b** and **4b** were determined. As expected, the *trans*-2,2 complexes (**1a** and **1b**) are lower in energy than the *cis*-2,2 complexes, with the energy differences being 31.7 kJ/mol and 32.4 kJ/mol, respectively. This difference in energy is small enough that the MeOH axial interaction with the Mo<sub>2</sub> core as well as hydrogen bonding between MeOH and the equatorial ligands seen in **4a** can be enough to make **4a** more thermodynamically favorable than **1a** when the compound is prepared in the presence of MeOH.

Diagrams of the metal frontier orbitals for complexes **1**, **2**, and **4** are shown in Figure 10. These MO diagrams show the same order of Mo≡Mo bonding and antibonding orbitals that has been found in other Mo<sub>2</sub>(thioamidate)<sub>4</sub> complexes.<sup>7,8a</sup> In complexes **1a**, **1b**, and **2**, the  $\pi$ -symmetry orbitals are degenerate, while in **4a** and **4b**, the  $\pi$ -symmetry orbitals lose their degeneracy. The loss of  $\pi$  degeneracy occurs due to a reduction of symmetry from idealized  $D_{2d}$  for the *trans*-2,2 regioisomer to  $C_{2h}$  for the *cis*-2,2 regioisomer. In the  $C_{2h}$  point group, the  $\pi$  orbitals are not equivalent by symmetry and hence are non-degenerate.

In each compound, the HOMO is the Mo≡Mo  $\delta$  orbital, and the LUMO is the Mo≡Mo  $\delta^*$  orbital. The HOMO-LUMO gap decreases depending on the  $\pi$ -basicity of the equatorial ligands. For the compounds with SNOX ligands, the HOMO-LUMO gap is approximately the same at  $\sim 3$  eV: Neither geometrical isomerism nor ligand sterics has much of an effect on the HOMO-LUMO gap. However, **2** with the SNS5 ligand has a HOMO-LUMO gap that is smaller than that of the SNOX compounds by about 0.4 eV. Ligand based  $\pi_{nb}$  orbitals have an antibonding interaction with the  $\delta^*$  LUMO of the *trans*-2,2 complexes. Since the SNS5 ligand has a more electron poor  $\pi$ -system than do the SNOX ligands (vide supra), SNS5 destabilizes the  $\delta^*$  orbital less than its SNOX counterparts, leading to the reduced HOMO-LUMO gap.

## Conclusions

The electronics of Mo<sub>2</sub>(thioamidate)<sub>4</sub> complexes can be tuned by changing the nature of the  $\pi$ -system substituents on the thioamidate ligands as well as altering the arrangement of the ligands around the Mo<sub>2</sub> core. Changing the  $\pi$ -system substituents from oxygen to sulfur reduces the amount of electron density that is available to the  $\pi$ -system of the ligand, which results in large changes to electronics of the Mo<sub>2</sub> core stabilized by the ligand. Upon substituting S for O as the  $\pi$ -system substituent, the Mo<sub>2</sub> core becomes more difficult to oxidize, the HOMO-LUMO

gap decreases, and the metal to ligand charge transfer becomes lower in energy by lowering the energy of the ligand-based  $\pi^*$  orbital. Changing the regioisomerism of the complex has a much smaller effect on the overall electronics. The increased steric clash between adjacent, uncoordinated O atoms in the *cis*-2,2 SNO equatorial ligands lengthens the metal ligand bonds, causing the ligands to be slightly less able to stabilize the Mo<sub>2</sub> core. This results in small increases in the electrochemical Mo<sub>2</sub><sup>4+/5+</sup> potential but minimal changes in the electronic structure of the compounds. Used in tandem, these two strategies could provide methods for the rational design of Mo<sub>2</sub>(thioamidate)<sub>4</sub> complexes that have precisely tuned electronic properties.

### Acknowledgements

We thank Ilia A. Guzei for his help in conducting the variable temperature crystallography experiment and Amanda R. Corcos for her help in collecting MALDI data as well as Momo Fredrickson and Daniel Fredrickson for providing us with the photograph of the violin in the TOC-graphic. The authors also wish to acknowledge financial support under NSF Grants CHE-1300464, CHE-9208463 (Bruker AC 360), and CHE-0840494 (computational facilities) as well as a generous bequest from Paul J. Bender (Bruker Avance 500).

### References

1. *Multiple Bonds between Metal Atoms*, ed. F. A. Cotton, C. A. Murillo, and R. A. Walton.; Springer Science and Business Media, New York, 3rd edn., 2005.
2. (a) W. Zhou, N. I. Saper, J. P. Krogman, B. M. Foxman, and C. M. Thomas. *Dalton Trans.* 2014, **43**, 1984. (b) J. W. Napoline, J. P. Krogman, R. Shi, S. Kuppuswamy, M. W. Bezpalko, B. M. Foxman, and C. M. Thomas, *Eur. J. Inorg. Chem.* 2013, 3874. (c) J. P. Krogman, M. W. Bezpalko, B. M. Foxman, and C. M. Thomas, *Inorg. Chem.* 2013, **52**, 3022. (d) J. W. Napoline, M. W. Bezpalko, B. M. Foxman, and C. M. Thomas, *Chem. Commun.* 2013, **49**, 4388. (e) A. R.

- Corcos, A. K. M. Long, I. A. Guzei, and J. F. Berry, *Eur. J. Inorg. Chem.* 2013, 3808. (f) M. Nippe, G. H. Timmer, and J. F. Berry, *Chem. Commun.*, 2009, 4357. (g) M. Nippe, E. Victor, and J. F. Berry, *Inorg. Chem.*, 2009, **48**, 11889. (h) A. K. M. Long, R. P. Yu, G. H. Timmer, and J. F. Berry, *J. Am. Chem. Soc.*, 2010, **132**, 12228. (i) M. Nippe, S. M. Goodman, C. G. Fry, and J. F. Berry, *J. Am. Chem. Soc.*, 2011, **133**, 2856. (j) A. K. M. Long, G. H. Timmer, J. S. Pap, J. L. Snyder, R. P. Yu, and J. F. Berry, *J. Am. Chem. Soc.*, 2011, **133**, 13138. (k) M. Nippe, Y. Turov, and J. F. Berry, *Inorg. Chem.*, 2011, **50**, 10592. (l) Y. Turov and J. F. Berry, *Dalton Trans.*, 2012, **41**, 8153. (m) G. H. Timmer and J. F. Berry, *Chem. Sci.*, 2012, **3**, 3038.
3. (a) K. P. Kornecki, D. C. Powers, T. Ritter, and J. F. Berry, *Prog. Inorg. Chem.* 2014, **58**, in press. (b) J. F. Berry, *Dalton Trans.* 2012, **41**, 700. (c) H. M. L. Davies and J. R. Manning, *Nature*, 2008, **451**, 417. (d) J. DuBois, *Org. Proc. Res. Dev.*, 2011, **15**, 758. (e) M. P. Doyle, R. Duffy, M. Ratnikov, and L. Zhou, *Chem. Rev.*, 2010, **110**, 704. (f) D. C. Powers and T. Ritter, *Acc. Chem. Res.*, 2012, **45**, 840. (g) L. Villalobos, Z. Cao, P. E. Fanwick, and T. Ren, *Dalton Trans.*, 2012, **41**, 644. (h) T. S. Teets and D. G. Nocera, *Chem. Commun.*, 2011, **47**, 9268. (i) A. Sinha, M. Majumdar, M. Sarkar, T. Ghatak, and J. K. Bera. *Organometallics*, 2013, **32**, 340.
4. (a) G. M. Chiarella, F. A. Cotton, J. C. Durivage, D. L. Lichtenberger, and C. A. Murillo. *J. Am. Chem. Soc.* 2013, **135**, 17889. (b) W. Zhou, S. L. Marquard, M. W. Bezpalko, B. M. Foxman, and C. M. Thomas *Organometallics*, 2013, **32**, 1766. (c) S.-A. Hua, Y.-C. Tsai, and S.-M. Peng, *J. Chin. Chem. Soc.* 2014, **61**, 9. (d) S. P. Cummings, J. Savchenko, P. E. Fanwick, A. Kharlamova, and T. Ren. *Organometallics*, 2013, **32**, 1129. (e) X. Xiao, C. Y. Liu, Q. He, M. J. Han, M. Meng, H. Lei, and X. Lu. *Inorg. Chem.*, 2013, **52**, 12624. (f) C. Y. Liu, X. Xiao, M. Meng, Y. Zhang, and M. J. Han. *J. Phys. Chem. C*, 2013, **117**, 19859. (g) X.-M. Cai, X.-Y. Zhang, J. Savchenko, Z. Cao, T. Ren, and J.-L. Zuo, *Organometallics*, 2012, **31**, 8591. (h) S. P.

Cummings, Z. Cao, P. E. Fanwick, A. Kharlamova, and T. Ren. *Inorg. Chem.* 2012, **51**, 7561. (i) W. P. Forrest, Z. Cao, K. M. Hassell, B. M. Prentice, P. E. Fanwick, and T. Ren. *Inorg. Chem.* 2012, **51**, 3261. (j) B. Xi, I. P.-C. Liu, G.-L. Xu, M. M. R. Choudhuri, M. C. DeRosa, R. J. Crutchley, and T. Ren. *J. Am. Chem. Soc.* 2011, **133**, 15094. (k) M. H. Chisholm, in *Structure and Bonding*, ed. G. Parkin, Springer, 2010, vol. 136, pp. 29-58. (l) M. H. Chisholm and N. S. Patmore, *Acc. Chem. Res.*, 2007, **40**, 19. (m) J. F. Berry, in *Structure and Bonding*, ed. G. Parkin, Springer, 2010, vol. 136, pp. 1-28. (n) P. J. Mohan, V. P. Georgiev, and J. E. McGrady, *Chem. Sci.*, 2012, **3**, 1319. (o) G. L. Manni, A. Dzubak, A. Mulla, D. W. Brogden, J. F. Berry, and L. Gagliardi, *Chem. Eur. J.*, 2012, **18**, 1737.

5. (a) D. C. Powers, M. B. Chambers, T. S. Teets, N. Elgrishi, B. L. Anderson, and D. Nocera. *Chem. Sci.* 2013, **4**, 2880. (b) T. S. Teets, M. P. Neumann, and D. G. Nocera. *Chem. Commun.* 2011, **47**, 1485. (c) T. S. Teets and D. G. Nocera. *J. Am. Chem. Soc.* 2011, **133**, 17796. (d) M. H. Chisholm, *Macromol. Chem. Phys.*, 2012, **213**, 800. (e) M. H. Chisholm and B. J. Lear, *Chem. Soc. Rev.*, 2011, **40**, 5254. (f) B. G. Alberding, M. H. Chisholm, J. C. Gallucci, Y. Ghosh, and T. L. Gustafson, *Proc. Nat. Acad. Sci. USA*, 2011, **108**, 8152. (g) P. M. Bradley, P. K.-L. Fu, and C. Turro, *Comments Inorg. Chem.* 2001, **22**, 393.

6. (a) S. J. Tereniak, R. K. Carlson, L. J. Clouston, V. G. Young, Jr., E. Bill, R. Maurice, Y.-S. Chen, H. J. Kim, L. Gagliardi, and C. C. Lu. *J. Am. Chem. Soc.* in press. (b) L. J. Clouston, R. B. Siedschlag, P. A. Rudd, N. Planas, S. Hu, A. D. Miller, L. Gagliardi, and C. C. Lu. *J. Am. Chem. Soc.* 2013, **135**, 13142. (c) P. A. Rudd, S. Liu, N. Planas, E. Bill, L. Gagliardi, and C. C. Lu. *Angew. Chem. Int. ed. Eng.* 2013, **52**, 4449. (d) Z. F. Tan, C. Y. Liu, Z. Li, M. Meng, and N. S. Weng. *Inorg. Chem.*, 2012, **51**, 2212. (e) P. A. Rudd, S. Liu, L. Gagliardi, V. G. Young, Jr., and C. C. Lu. *J. Am. Chem. Soc.* 2011, **133**, 20724. (f) A. S. Filatov, M. Napier, V. D. Vreshch, N. J.

- Sumner, E. V. Dikarev, and M. A. Petrukhina, *Inorg. Chem.*, 2012, **51**, 566. (g) A. S. Filatov and M. A. Petrukhina, *Coord. Chem. Rev.*, 2010, **254**, 2234. (h) M. Majumdar, S. K. Patra, J. K. Bera. *Polyhedron*, 2006, **26**, 1597. (i) M. H. Chisholm and A. M. Macintosh, *Chem. Rev.*, 2005, **105**, 2949. (j) D. R. Manke, Z.-H. Loh, and D. G. Nocera. *Inorg. Chem.* 2004, **43**, 3618. (k) F. A. Cotton, C. Lin, and C. A. Murillo, *Acc. Chem. Res.*, 2001, **34**, 759.
7. J. Hicks, S. P. Ring, and N. J. Patmore, *Dalton Trans.*, 2012, **41**, 6641.
8. (a) B. S. Dolinar and J. F. Berry, *Inorg. Chem.*, 2013, **52**, 4658. (b) F. A. Cotton, R. H. Niswander, and J. C. Sekutowski. *Inorg. Chem.*, 1979, **18**, 1149. (c) H. P. M. M. Ambrosius, F. A. Cotton, L. R. Falvello, H. T. J. M. Hintzen, T. J. Melton, W. Schwotzer, M. Tomas, and J. G. M. van der Linden, *Inorg. Chem.*, 1984, **23**, 1611. (d) P. E. Fanwick, J.-S. Qi, Y.-P. W, and R. A. Walton, *Inorg. Chim. Acta*, 1990, **168**, 159. (e) W. S. Sheldrick and M. Mintert, *Inorg. Chim. Acta*, 1994, **219**, 23.
9. (a) F. A. Cotton, R. H. Niswander, and J. C. Sekutowski, *Inorg. Chem.*, 1979, **18**, 1152. (b) F. A. Cotton, W. H. Ilsley, and W. Kaim, *J. Am. Chem. Soc.*, 1980, **102**, 3475. (c) A. Bing, F. A. Cotton, and W. Kaim, *Inorg. Chem.*, 1979, **18**, 3030. (d) F. A. Cotton, W. H. Ilsley, and W. Kaim, *Inorg. Chem.* 1980, **19**, 1453. (e) S. Baral, F. A. Cotton, W. H. Ilsley, and W. Kaim, *Inorg. Chem.*, 1982, **21**, 1644. (f) W. Clegg, C. D. Garner, and L. Akhter, M. H. Al-Samman, *Inorg. Chem.*, 1983, **22**, 2466. (g) D. L. Lichtenberger, J. G. Kristofzski, and M. A. Bruck, *Acta Crystallogr., Sect. C: Cryst. Struct. Commun.*, 1988, **C44**, 1523. (h) R. G. Abbott, F. A. Cotton, and L. R. Falvello, *Inorg. Chem.*, 1990, **29**, 514. (i) K. Mashima, H. Nakano, T. Mori, H. Takaya, and A. Nakamura, *Chem. Lett.*, 1992, 185. (j) M. Mintert and W. S. Sheldrick, *Chem. Ber.*, 1996, **129**, 683. (k) K. Pal, K. Nakao, and K. Mashima, *E. J. Inorg. Chem.*, 2010, 5668. (l)

- L. A. Wilkinson, L. McNeill, P. A. Scattergood, and N. J. Patmore, *Inorg. Chem.*, 2013, **52**, 9683.
10. G. Holste and H. Schäfer, *Z. anorg. allg. Chem.*, 1972, **391**, 263.
11. F. A. Cotton and G. J. Norman, *J. Coord. Chem.*, 1971, **1**, 161.
12. U. Berg and J. Sandström, *Acta Chemica Scandinavica*, 1966, **20**, 689.
13. X. Zhu, T. Giordano, Q. -S. Yu, H. W. Holloway, T. A. Perry, D. K. Lahiri, A. Brossi, and N. H. Greig, *J. Med. Chem.*, 2003, **46**, 5222.
14. SMART; Bruker-AXS: Madison, WI, 2009.
15. G. M. Sheldrick, *Acta Crystallogr., Sect. A: Found. Crystallogr.*, 2008, **A64**, 112.
16. (a) Neese, F. ORCA-an ab initio DFT and Semi-empirical Electronic Structure Package, version 2.8.0; University of Bonn: Germany, 2010. (b) J. P. Perdew, *Phys. Rev. B: Condens. Matter*, 1986, **33**, 8822. (c) A. D. Becke, *Phys. Rev. A: At. Mol. Opt.* 1988, **38**, 3098.
17. F. Weigend and R. Ahlrichs, *Phys. Chem. Chem. Phys.*, 2005, **7**, 3297.
18. The  $^{13}\text{C}$  NMR of **4a** also is distinct from that of **1a**. We reported previously<sup>8a</sup> the  $^{13}\text{C}$  NMR spectra of **1a**, but in the course of the work described in this paper, we realized that our reported  $^{13}\text{C}$  spectrum of **1a** also contained as well as possibly the 3,1 isomer. Our previous report therefore notes additional (erroneous) peaks. We have been unable to obtain perfectly clean spectra of **1a**, but the  $^{13}\text{C}$  signals of **1a** are clearly the following:  $\delta$  215.65, 186.96, 39.55, 32.30.
19. The *trans*-1,1 notation refers to a paddlewheel complex having two different equatorial ligands, one of which has asymmetric donor atoms (e.g. N, S). The asymmetric ligands are *trans* to each other with their donor atoms oriented in opposite directions along the Mo $\equiv$ Mo vector. For further discussion of this, see reference 9(l).

Figure

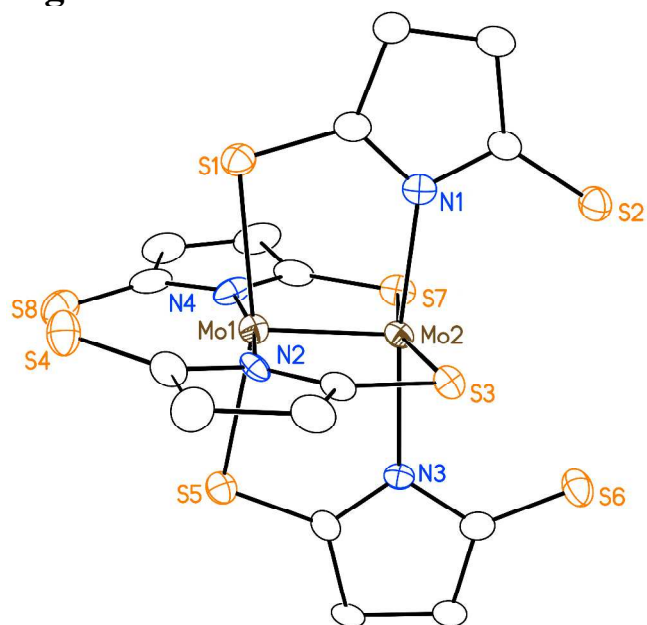


**Figure 1.** The crystal structure of *trans*-2,2-Mo<sub>2</sub>(SNS5)<sub>4</sub> (**2**). All atoms are drawn as 50% probability thermal ellipsoids. All hydrogen atoms and solvents of crystallization are omitted for clarity. The compound crystallizes with a molecule of CH<sub>2</sub>Cl<sub>2</sub> in the asymmetric unit.

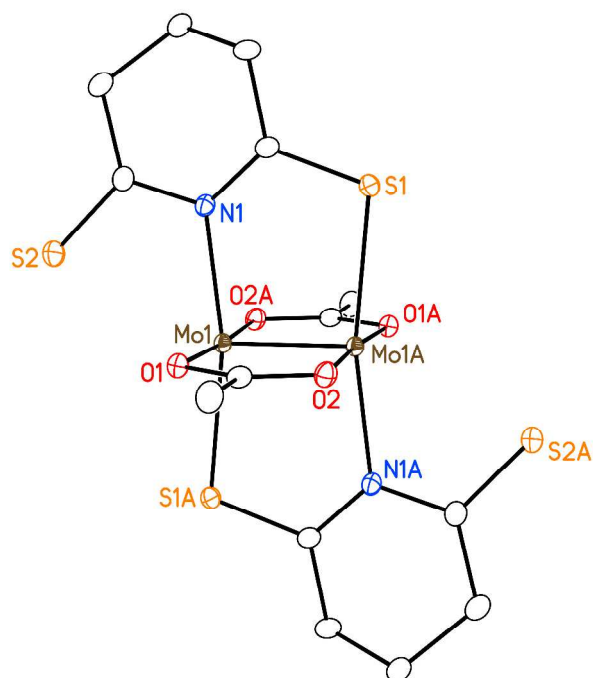


**Figure 2.** The crystal structure of *trans*-1,1-Mo<sub>2</sub>(OAc)<sub>2</sub>(SNS6)<sub>2</sub> (**3**). All atoms are drawn as 50% probability thermal ellipsoids. All hydrogen atoms are omitted for clarity.

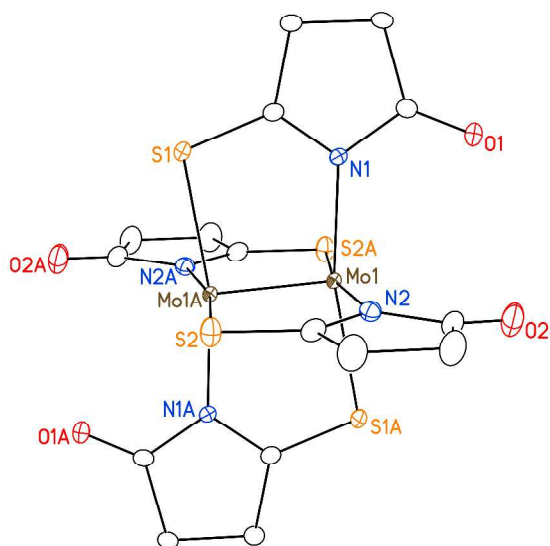


**Figure 3.** The crystal structure of *cis*-2,2-Mo<sub>2</sub>(SNO<sub>5</sub>)<sub>4</sub> (**4a**). All atoms are drawn as 50% probability thermal ellipsoids. All hydrogen atoms are omitted for clarity.

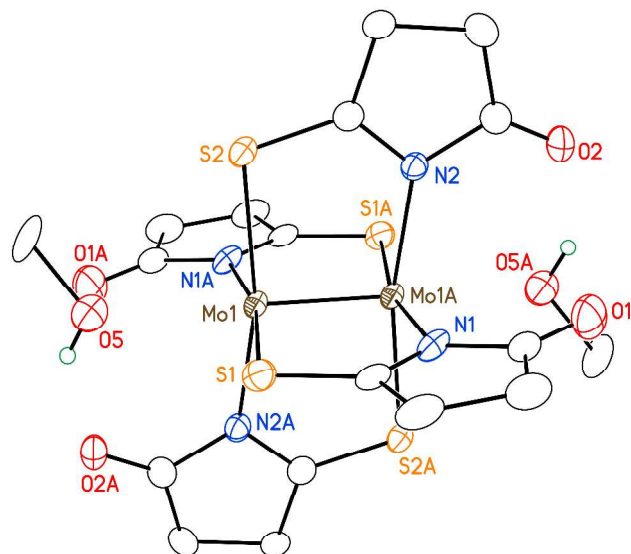


**Figure 4.** The 100 K crystal structure of one molecule of **4a**·2MeOH. All atoms are drawn as 50% probability thermal ellipsoids. All hydrogen atoms except those of the MeOH solvate are omitted for clarity.

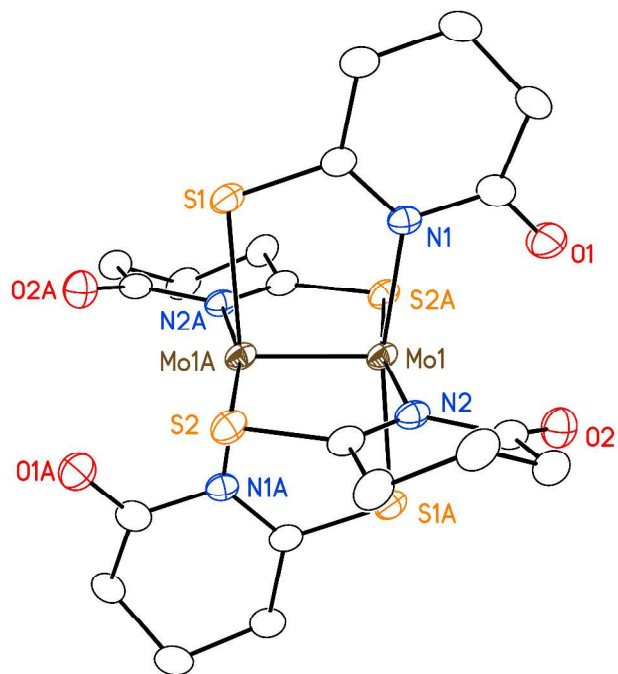


**Figure 5.** The X-ray crystal structure of *cis*-2,2-Mo<sub>2</sub>(SNO<sub>6</sub>)<sub>4</sub> (**4b**). All atoms are drawn as 50% probability thermal ellipsoids. All hydrogen atoms and solvent molecules are omitted for clarity.

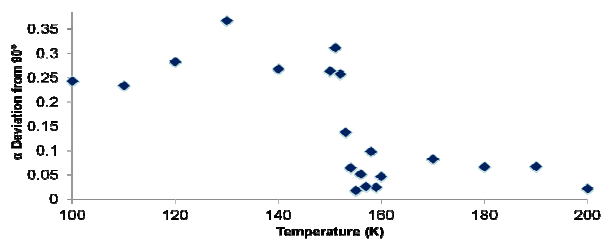


**Figure 6.** The temperature dependence of the deviation of the  $\alpha$  unit cell parameter from  $90^\circ$  of  $4a \cdot \text{MeOH}$ . This is an unconstrained parameter.

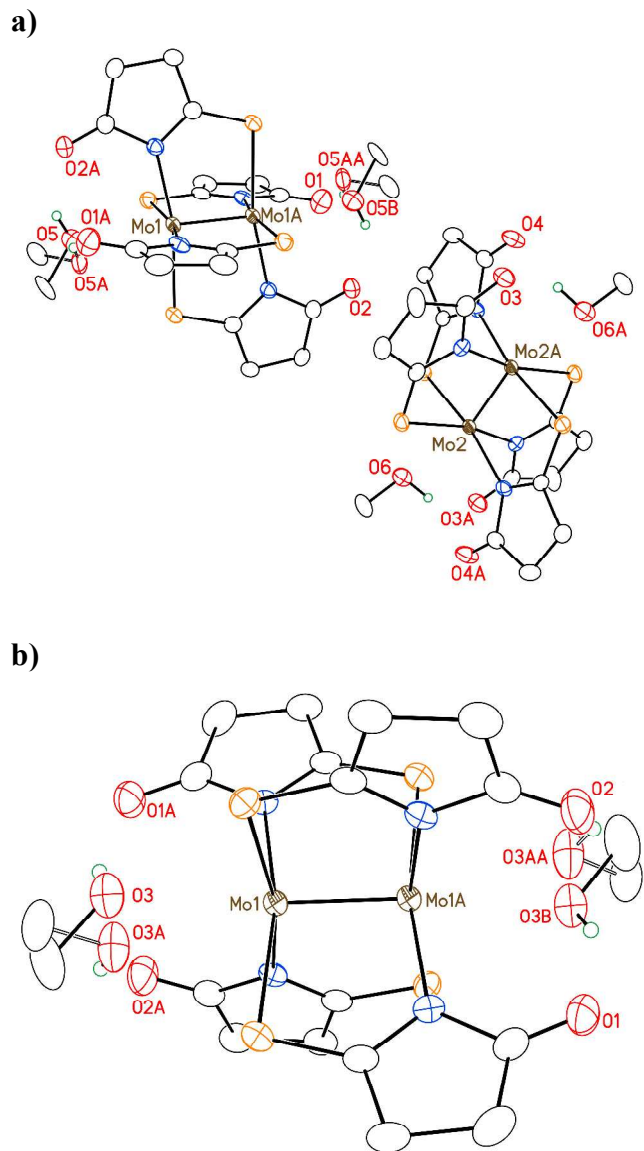


**Figure 7.** A comparison of the (a) 100 K and (b) 200 K structures of **4a**, illustrating the disorder present in both complexes. The atoms are drawn as either 50% (100 K) or 40% (200 K) thermal ellipsoids. All hydrogen atoms, except those on the MeOH solvate molecules have been omitted for clarity.

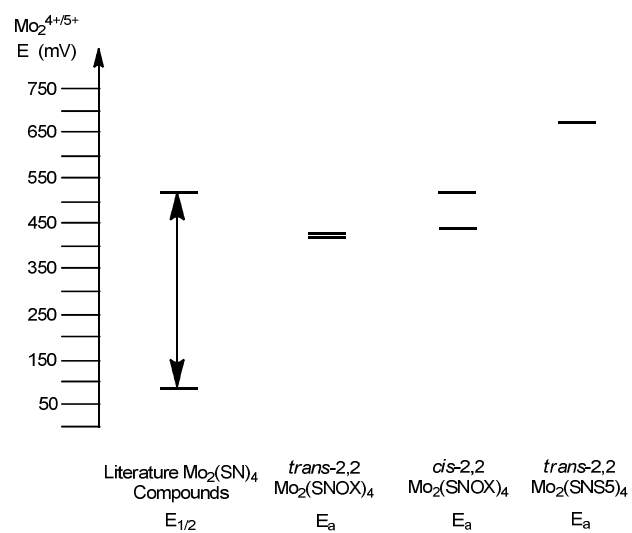


**Figure 8.** A comparison of the oxidation potentials of Mo<sub>2</sub>(SN)<sub>4</sub> complexes.

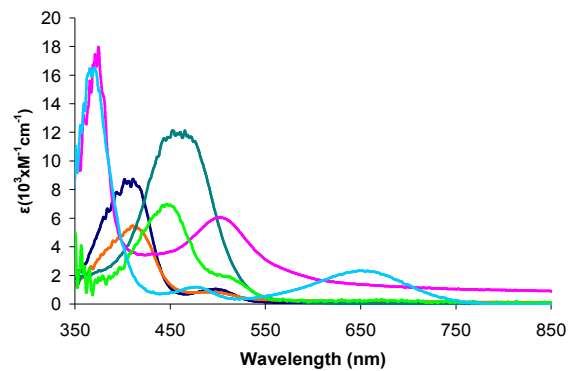


**Figure 9.** The UV-vis spectra of **1-4**. Compound **1a** is navy, **1b** is teal, **2** is pink, **3** is light blue, **4a** is orange, **4b** is green.

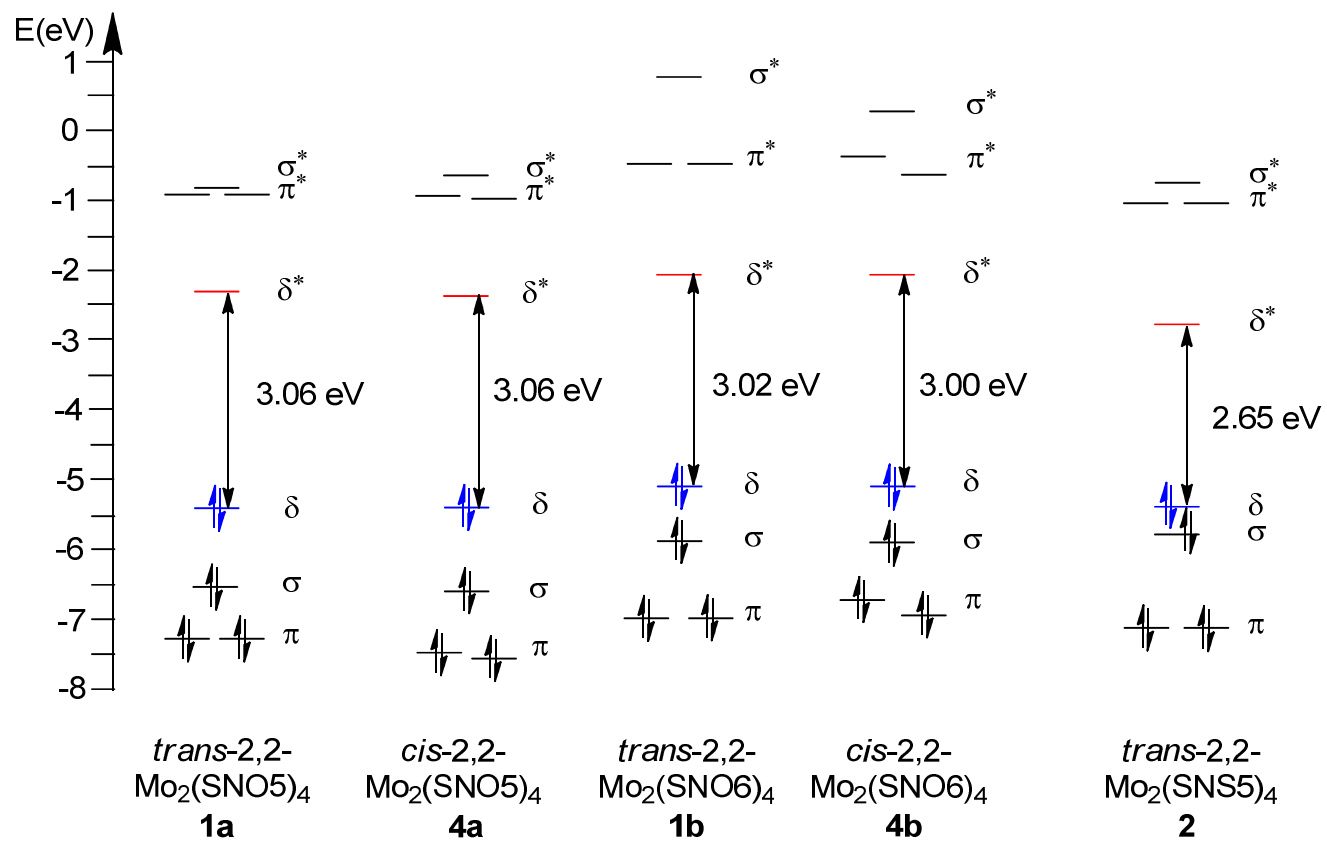


**Figure 10.** The metal-based MO diagrams of compounds **1-4** with orbital energies based on the results of DFT (B3LYP) calculations.

## Tables

Table 1. The crystallographic details of compounds 1-4.

Compound	2	3	4a·CH <sub>2</sub> Cl <sub>2</sub>	4a·2MeOH	4a·2MeOH	4b·2 1,2-DCE
<b>Empirical formula</b>	C <sub>17</sub> H <sub>18</sub> Cl <sub>2</sub> Mo <sub>2</sub> N <sub>4</sub> S <sub>8</sub>	C <sub>14</sub> H <sub>18</sub> Mo <sub>2</sub> N <sub>2</sub> O <sub>4</sub> S <sub>4</sub>	C <sub>18</sub> H <sub>20</sub> Cl <sub>4</sub> Mo <sub>2</sub> N <sub>4</sub> O <sub>4</sub> S <sub>4</sub>	C <sub>18</sub> H <sub>24</sub> Mo <sub>2</sub> N <sub>4</sub> O <sub>6</sub> S <sub>4</sub>	C <sub>18</sub> H <sub>24</sub> Mo <sub>2</sub> N <sub>4</sub> O <sub>6</sub> S <sub>4</sub>	C <sub>24</sub> H <sub>32</sub> Cl <sub>4</sub> Mo <sub>2</sub> N <sub>4</sub> O <sub>4</sub> S <sub>4</sub>
<b>Formula weight</b>	797.61	598.42	818.30	712.53	712.53	902.46
<b>Temperature/K</b>	100(1)	100(1)	100(1)	100(1)	200(1)	100(1)
<b><math>\lambda/\text{\AA}</math></b>	0.71073	0.71073	0.71073	0.71073	1.54178	0.71073
<b>Crystal system</b>	monoclinic	monoclinic	monoclinic	triclinic	monoclinic	monoclinic
<b>Space group</b>	<i>P2<sub>1</sub>/c</i>	<i>P2<sub>1</sub>/c</i>	<i>P2<sub>1</sub>/c</i>	<i>P</i> <b>1</b>	<i>P2<sub>1</sub>/c</i>	<i>P2<sub>1</sub>/c</i>
<b><i>a</i>/\AA</b>	16.322(6)	8.4950(2)	9.101(4)	8.990(3)	9.0133(5)	9.7312(2)
<b><i>b</i>/\AA</b>	10.791(4)	7.4672(2)	20.55(1)	14.717(7)	14.716(1)	9.0334(2)
<b><i>c</i>/\AA</b>	16.081(7)	15.4637(4)	7.445(4)	10.048(4)	10.0976(7)	19.1659(4)
<b><math>\alpha</math>/°</b>	90	90	90	89.65(2)	90	90
<b><math>\beta</math>/°</b>	105.44(3)	104.634(1)	110.31(2)	112.53(1)	111.403(4)	103.771(1)
<b><math>\gamma</math>/°</b>	90	90	90	88.73(2)	90	90
<b>Volume/\AA<sup>3</sup></b>	2730(2)	949.10(4)	1306(1)	1227.6(9)	1247.0(2)	1636.36(6)
<b>Z</b>	4	2	2	2	2	2
<b><math>\rho_{\text{calc}}</math>/mg/mm<sup>3</sup></b>	1.940	2.094	2.081	1.928	1.898	1.832
<b>2<math>\theta</math> range for data collection</b>	2.588 to 51.884°	4.96 to 61.08°	3.964 to 54.952°	7.014 to 55.056°	10.542 to 144.784°	4.3 to 63.22°
<b>Independent reflections</b>	5323	2908	2981	8926	2451	5496
<b>R(int)</b>	0.0599	0.0549	0.0542	0.0618	0.0219	0.0408
<b>Data/restraints/parameters</b>	5323/0/298	2908/0/119	2981/10/173	8926/0/336	2451/39/180	5496/0/217
<b>Goodness-of-fit on F<sup>2</sup></b>	1.296	1.099	1.060	0.978	1.060	1.048
<b>Final R indexes</b>	R <sub>1</sub> = 0.0480	R <sub>1</sub> = 0.0241	R <sub>1</sub> = 0.0366	R <sub>1</sub> = 0.0516,	R <sub>1</sub> = 0.0182	R <sub>1</sub> = 0.0220
<b>[I ≥ 2<math>\sigma</math>(I)]<sup>a,b</sup></b>	wR <sub>2</sub> = 0.1090	wR <sub>2</sub> = 0.0551	wR <sub>2</sub> = 0.0833	wR <sub>2</sub> = 0.1176	wR <sub>2</sub> = 0.0447	wR <sub>2</sub> = 0.0551
<b>Final R indexes [all data]</b>	R <sub>1</sub> = 0.0658	R <sub>1</sub> = 0.0326	R <sub>1</sub> = 0.0509	R <sub>1</sub> = 0.0740	R <sub>1</sub> = 0.0196	R <sub>1</sub> = 0.0293
	wR <sub>2</sub> = 0.1167	wR <sub>2</sub> = 0.0573	wR <sub>2</sub> = 0.0884	wR <sub>2</sub> = 0.1269	wR <sub>2</sub> = 0.0453	wR <sub>2</sub> = 0.0577

<sup>a</sup>R<sub>1</sub> =  $\sum ||F_o| - |F_c|| / \sum |F_o|$ . <sup>b</sup>wR<sub>2</sub> =  $[\sum [w(F_o^2 - F_c^2)^2] / \sum [w(F_o^2)^2]]^{1/2}$ , w =  $1/\sigma^2(F_o^2) + (aP)^2 + bP$ , where P =  $[\max(0 \text{ or } F_o^2) + 2(F_c^2)]/3$ .

**Table 2.** The relevant bond distances for Compounds **1-4**

Compound	Mo-Mo (Å)		Mo-N (Å)		Mo-S (Å)		Reference
	Exp.	DFT	Exp.	DFT	Exp.	DFT	
<b>1a</b>	2.1112(4)	2.0862	2.145[2]	2.1493	2.4753[8]	2.5231	8a
<b>1b</b>	2.1150(2)	2.0746	2.153[3]	2.2167	2.481[8]	2.5379	8a
<b>2</b>	2.1242(6)	2.1336	2.155[6]	2.1482	2.485[2]	2.4925	This work
<b>3</b>	2.108(2)	-	2.160(2)	-	2.4813(6)	-	This work
<b>4a</b>	2.145(2)	2.0824	2.166[3]	2.1597	2.496[2]	2.5206	This work
<b>4a</b> ·MeOH (100 K)	2.153[2]	2.1313	2.164[5]	2.1868	2.499[2]	2.5116	This work
<b>4a</b> ·MeOH (200 K)	2.1408(3)		2.159[2]		2.4942[5]		This work
<b>4b</b>	2.1061(2)	2.0832	2.162[2]	2.1917	2.4790[4]	2.5016	This work

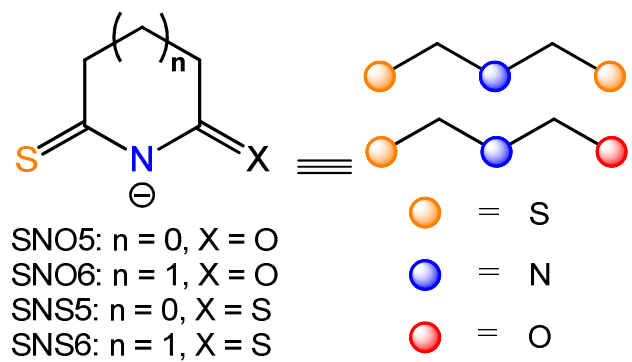
**Table 3.** The  $E_{1/2}$  and  $E_a$  of the  $\text{Mo}_2(\text{SN})_4$  compounds studied in this project. All potentials are referenced to  $\text{Fc}/\text{Fc}^+$  couple.

<b>Compound</b>	<b><math>E_{1/2}</math> (mV)</b>	<b><math>E_a</math> (mV)</b>	<b>Solvent</b>	<b>Reference</b>
<i>trans</i> -2,2- $\text{Mo}_2(\text{SNS5})_4$ ( <b>3</b> )	–	693	$\text{CH}_2\text{Cl}_2$	This work
<i>cis</i> -2,2- $\text{Mo}_2(\text{SNO5})_4$ ( <b>4a</b> )	–	520	$\text{CH}_2\text{Cl}_2$	This work
<i>cis</i> -2,2- $\text{Mo}_2(\text{SNO6})_4$ ( <b>4b</b> )	–	443	$\text{CH}_2\text{Cl}_2$	This work
<i>trans</i> -2,2- $\text{Mo}_2(\text{SNO5})_4$ ( <b>1a</b> )	388	425	MeCN	8a
<i>trans</i> -2,2- $\text{Mo}_2(\text{SNO6})_4$ ( <b>1b</b> )	351	415	$\text{CH}_2\text{Cl}_2$	8a

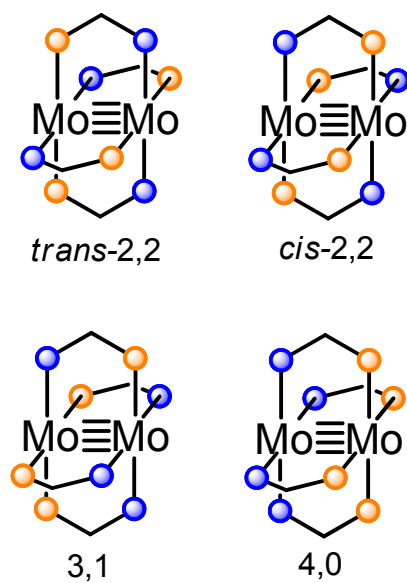
**Table 4.** The peak wavelength and extinction coefficients of **1 - 4**.

Transition	<b>L<math>\pi</math>-L<math>\pi^*</math></b>		<b><math>\delta</math>-L <math>\pi^*</math></b>		<b><math>\delta</math>-<math>\delta^*</math></b>	
	<b>Compound</b>	<b><math>\lambda_{\max}</math> (nm)</b>	<b><math>\epsilon</math> (<math>M^{-1}cm^{-1}</math>)</b>	<b><math>\lambda_{\max}</math> (nm)</b>	<b><math>\epsilon</math> (<math>M^{-1}cm^{-1}</math>)</b>	<b><math>\lambda_{\max}</math> (nm)</b>
<b>1a</b>	–	–	414	5400	495	830
<b>1b</b>	–	–	460	12000	–	–
<b>2</b>	375	17000	505	5100	–	–
<b>3</b>	371	17000	648	2400	477	1200
<b>4a</b>	–	–	410	8600	498	1100
<b>4b</b>	–	–	449	6900	502	2100

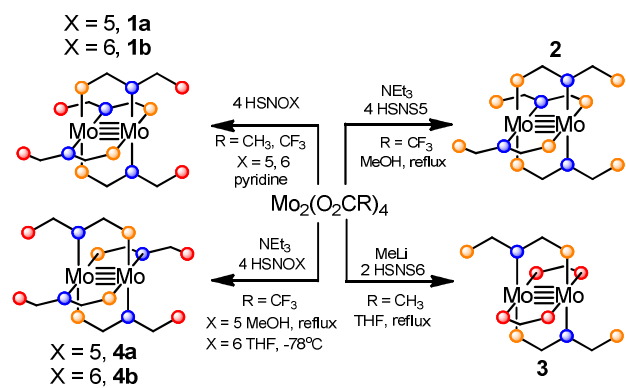
## Schemes



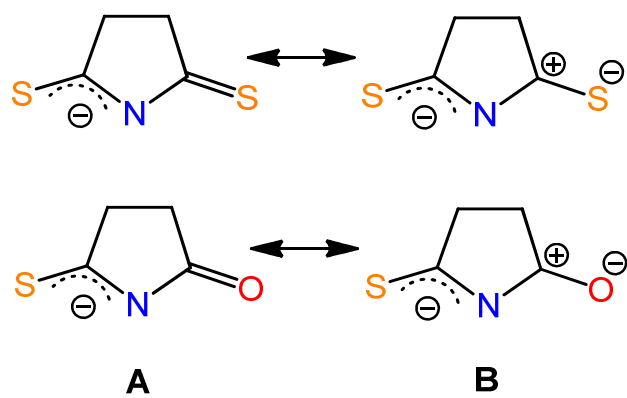
**Scheme 1.** The ligands used in this project.



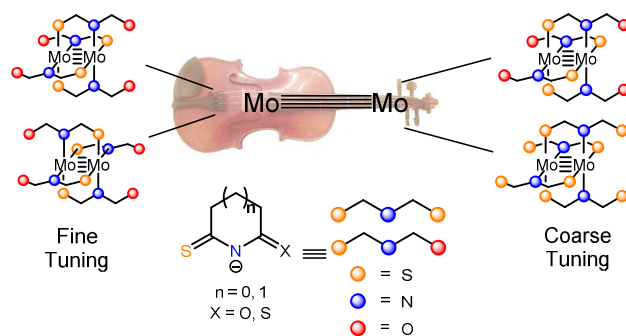
**Scheme 2.** The regioisomers of  $\text{Mo}_2(\text{thioamidate})_4$  complexes.



**Scheme 3.** The syntheses of a)  $\text{Mo}_2(\text{SNOX})_4$  complexes and b)  $\text{Mo}_2(\text{SNSX})$  complexes.



**Scheme 4.** The resonance structures of SNS5 and SNO5 ligands.



Reported here are the syntheses and characterizations of new  $\text{Mo}_2(\text{thioamidate})_4$  complexes. By varying the  $\pi$ -system substituent and regioisomerism of these compounds, their electronics are tuned with varying degrees of effect.